International Journal of Nanomedicine Dovepress

Open Access Full Text Article ORIGINAL RESEARCH

Injectable Polyhydroxyalkanoate-Nano-Clay Microcarriers Loaded with r-BMSCs Enhance the Repair of Cranial Defects in Rats

Hai Ci[1–3,*], Junjin Jie[1,2,*], Guo Zhang[1,2], Linping Wu[4], Zhenxing Wang[1,2], Jiaming Sun[1,2]

[1]Department of Plastic Surgery, Union Hospital, Tongji Medical College, Huazhong University of Science and Technology, Wuhan, 430022, People's Republic of China; [2]Wuhan Clinical Research Center for Superficial Organ Reconstruction, Wuhan, 430022, People's Republic of China; [3]Department of Burn and Plastic Surgery, The First Affiliated Hospital of Shihezi University, Shihezi, 8320082, People's Republic of China; [4]Key Laboratory of Immune Response and Immunotherapy, China-New Zealand Joint Laboratory of Biomedicine and Health, Guangdong Provincial Key Laboratory of Biocomputing, Guangzhou Institutes of Biomedicine and Health, Chinese Academy of Sciences, Guangzhou, 510530, People's Republic of China

*These authors contributed equally to this work

Correspondence: Zhenxing Wang; Jiaming Sun, Email benjamin.wzx@163.com; Sunjm1592@sina.com

Purpose: Successful regeneration of cranial defects necessitates the use of porous bone fillers to facilitate cell proliferation and nutrient diffusion. Open porous microspheres, characterized by their high specific surface area and osteo-inductive properties, offer an optimal microenvironment for cell ingrowth and efficient ossification, potentially accelerating bone regeneration.

Materials and Methods: An in vitro investigation was conducted to assess the physicochemical properties, porosity, and biocompatibility of PHA-nano-clay open porous microspheres. Subsequently, PHA-nano-clay microspheres loaded with rat bone marrow mesenchymal stem cells were implanted into 5 mm cranial defects in rats for a duration of 12 weeks and were evaluated through histological and immunohistochemical analyses.

Results: The incorporation of nano-clay into PHA resulted in improved mechanical properties of the porous scaffolds. Furthermore, cell adhesion, viability, and morphology on the scaffolds were maintained. The PHA-3% nano-clay open porous microspheres effectively enhanced the repair of cranial defects compared to the control group, without recurrence or complications.

Conclusion: Porous PHA-nano-clay microspheres, with their high specific surface area, biodegradability, and osteo-inductive properties, can be utilized as a bone-filling material for improved bone defect repair through cell delivery. In particular, PHA-3% nano-clay open porous microspheres exhibit promising therapeutic potential in the repair of cranial defects.

Keywords: P34HB, open porous microspheres, bone-filling biomaterial, osteo-inductivity, cranial defects

Introduction

Cranial defects are a prevalent complication in patients with trauma and surgical interventions, impacting a significant number of individuals worldwide.[1–4] The high incidence of cranial defect syndrome and secondary brain injuries emphasizes the importance of prompt skull repair.[5] Despite the variety of cranial defect repair materials currently available, they still do not adequately address the clinical demands, necessitating multiple invasive surgeries and extensive reshaping.[2,6,7] Autogenous bone grafts are susceptible to absorption, difficult to store, and have a high risk of infection.[8] Silicone rubber materials, due to their electrostatic properties, readily attract foreign particles, triggering postoperative foreign body reactions.[6] Metallic materials like titanium mesh conduct heat and electricity, which may lead to chronic brain tissue damage due to temperature fluctuations.[6,9,10] Therefore, it is of vital importance to develop new regenerative materials that promote cranial bone repair.

An injectable bone filler should ideally be highly porous to support rapid cell ingrowth and vascularization, thereby accelerating the repair process.[5,11,12] Biodegradable microspheres have emerged as one of the most promising injectable micro-scaffolds that have a higher specific surface area than bulk scaffolds, improved nutrient diffusion, and flexibility in

Received: 22 October 2024
Accepted: 4 December 2024
Published: 24 December 2024

Graphical Abstract

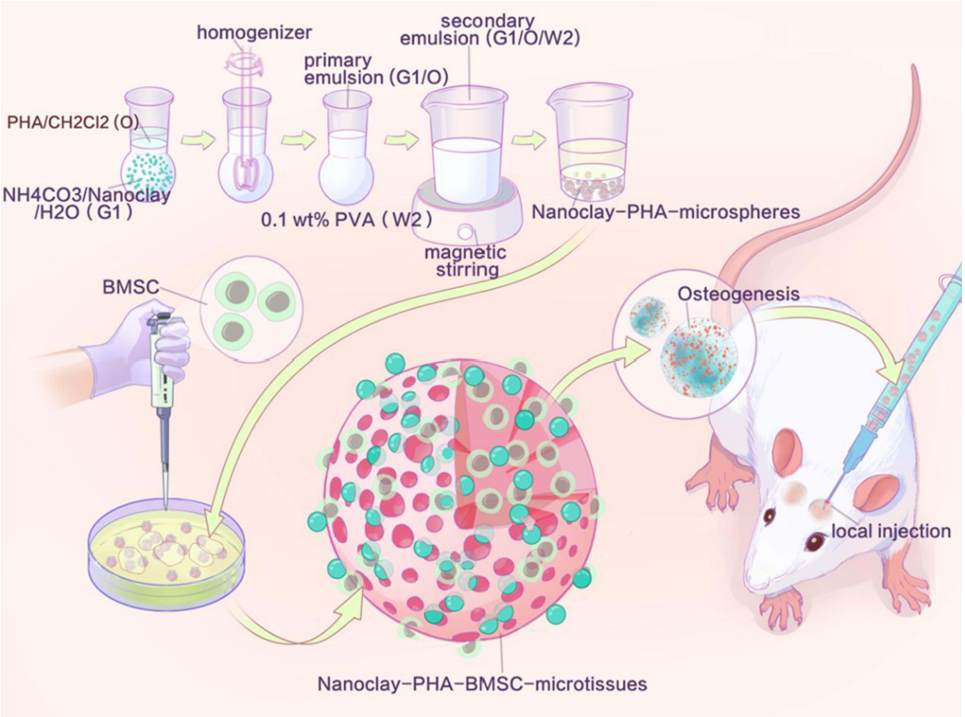

assembly.[13–15] Porous microspheres feature interconnected porous structures, which makes them suitable for injection and cell/tissue ingrowth.[16,17] Porous microspheres have the advantage of being injectable and may reduce cell damage during injection when serving as cell carriers for implantation.[11,13] Porous microspheres can also improve the regeneration of injured bone tissue by providing various biophysical and biochemical cues for cell fate modulation.[5,18,19] Herein, we focused on the highly porous microspheres with sufficient internal space for cell proliferation and nutrient diffusion to aid in tissue defect reconstruction.[11,20]

The biocompatibility and mechanical properties of biomaterials are the foundation for porous microspheres to facilitate cranial defect repair. Biodegradable synthetic polymers, including polylactide (PLA) and polycaprolactone (PCL), are unsuitable for guided bone regeneration due to acidic degradation products.[21] Polyhydroxyalkanoate (PHA), a family of bio-polyesters produced by many bacteria, is increasingly used to create matrices for drug delivery and encapsulation and for cell and tissue regeneration.[11,22,23] A previous study reported that Poly 4-hydroxybutyrate(P4HB)-based growth factor-free OPMs can enhance osteoblast differentiation of bone marrow mesenchymal stem cells (BMSCs) in vitro and accelerate rat skull cranial defects recovery.[11] Poly(3-hydroxybutyrate-co-4-hydroxybutyrate) (P34HB), a type of PHA, exhibits excellent biocompatibility and serves as a potential biomaterial for cranial bone repair.[24–29]

Nano-clay particles (NP) are emerging as intriguing 2D nanomaterials for bone tissue engineering with multiple functions, including improving mechanical properties and intrinsic osteo-inductivity.[30,31] NP can induce osteogenic differentiation of human mesenchymal stem cells in vitro without the use of any other osteo-inductive factors.[32,33] This pro-osteoblastic activity of NP may be due to nontoxic degradation products, such as Li, $Si(OH)_4$, and Mg^{2+}, and the interactions with cellular components.[34] BMSCs were chosen as seeding cells because of their proven multipotent differentiation potential, particularly down the osteogenic lineage, availability, and proliferative capacity in vitro.[16,35,36] Additionally, rat bone marrow mesenchymal stem cells (r-BMSCs) interact through paracrine signaling processes to modulate host cell behavior and the inflammatory response, potentially promoting a favorable regenerative outcome.[16,20,36]

Incorporating NP into the porous PHA microspheres is an ideal strategy for enhanced bone regeneration to mimic the organic-inorganic nature of the bone extracellular matrix (ECM). PHA-NP OPMs have high water uptake ratio and porosity, facilitating in- and out-transport of oxygen, nutrients, and metabolic wastes, thereby promoting cell proliferation on and inside the microspheres.[37,38] Open porous microspheres (OPMs) combined the advantages of PHA porous microspheres and NP to serve as injectable carriers for proliferating stem cells.[39,40] Accordingly, injectable PHA-NP OPMs are promising candidates for cranial defect tissue engineering. This study investigated the osteogenic potential of injectable PHA and NP composite OPMs for r-BMSC delivery in vitro and in vivo. The regenerative potentials of PHA-NP OPMs were assessed in vivo in 5 mm rat critical-size cranial defects for 4 and 12 weeks.

Materials and Methods

r-BMSCs Isolation and in vitro Culture

r-BMSCs were isolated and collected according to the previous description. This study was approved by the animal ethics committee of Tongji Medical College, Huazhong University of Science & Technology (Wuhan, China). Sacrifice of animals was consistent with state regulations and laws and in accordance with the Standing Committee on Ethics in China (State Scientific and Technological Commission of China). The protocol was approved by the ethical committee (approval number: 2019- S1154).

In brief, the neonate Sprague Dawley (SD) rats (3–5 days old) were given cervical dislocation for euthanasia, followed by soaking in 75% alcohol for 20 min. Muscles and soft tissues attached onto femurs and tibias were removed. Then, cartilages at both ends of the bones were cut off, and cavities were rinsed by culture medium three times till they were white. Later, the fresh bone marrow tissues were seeded on 10 cm culture dishes with culture medium (DMEM containing 10% fetal bovine serum (FBS) and 1% penicillin and streptomycin). Afterwards, r-BMSCs were cultured under 37 °C with 5% CO_2, and the culture medium was changed every 2 days. After r-BMSCs achieved confluency, the r-BMSCs were passaged.

Preparations of PHA OPMs

P34HB (P(3HB-co-4HB)) OPMs were prepared by an improved method of gas-in-oil-in-water (G1/O/W2) double emulsion assisted with releases of carbon dioxide and ammonia from ammonium bicarbonate degradation.[41] In detail, 1.5 g of P34HB (Bluepha, China) was dissolved in 30 mL methylene chloride (Sinopharm, China) to form 5 wt% concentration of the oil phase (O). The gas phase (G1) of pro-aqueous solution contains 15 g of ammonium bicarbonate (Sinopharm, China) and 100 mL of de-ionized water. About 5 mL of phase G1 and 15 mL of aforementioned PHA/methylene chloride solution (phase O) were mixed to form primary emulsion (G1/O) using a homogenizer (SUNNE, China) for 2 min. Subsequently, the primary emulsion was added dropwise to 100 mL of 0.1 wt% PVA (polyvinyl alcohol, Sigma, USA) solution under magnetic stirring (IKA, RCT, Germany) to form a secondary emulsion (G1/O/W2), which was continuously stirred for at least 5 hours, to allow complete evaporation of the methylene chloride. PLA and PCL OPMs were produced by the same aforementioned method described previously.[41] Traditional PHA solid microspheres (PHA SMs) as a control were also prepared by double emulsification using water as a pore-foaming agent. All the above generated PHA OPMs and SMs, as well as PLA and PCL microspheres were washed four times using at least 2000 mL de-ionized water to completely remove residual PVA.

Nile Red Staining and Fluorescence Measurement

Dissolve 10mg Nile red powder in 10mL of methanol solution makes a storage solution at the concentration of 1mg/mL. Phosphate Buffered Saline (PBS) was used to dilute the storage solution up to 100 times to make a working solution. The Nile red working solution was added to the microspheres and then stained at room temperature for 10 mins. Microspheres were washed 3 times with PBS to remove residual Nile red.

In vitro Cell Adhesion and Proliferation

CCK8

R-BMSCs were employed to investigate the cell behavior on the surface and in the internal space of OPMs. The cell activity during proliferation was studied with CCK-8 Kit. At each time point, the medium in each well was substituted with cell counting kit-8 working solution (CCK-8, biosharp, China), and OD values were read on a microplate reader.

Cell Cytocompatibility

For evaluation of the cytocompatibility of the microspheres, 10 mg dry microspheres were transferred to 48-well tissue culture plates (TCPs, Corning, USA) coated with 1% sterile agarose (Sigma, USA). Agarose effectively separated cells and TCPs, promoting cell adherence on microspheres and avoiding non-specific cell proliferation on TCPs. Prior to the cell cultivation, microspheres were sterilized via immersing the microspheres in 75 vol% ethanol overnight. Subsequently, all microspheres were washed at least three times with phosphate-buffered saline (PBS) and at least three times with culture medium without FBS. Each well (n = 6) was seeded with $2\times10^{\wedge6}$ r-BMSCs in 1mL of culture medium. The plates containing scaffolds were cultured in an incubator at 5% CO2, 37 °C. After 6 h of incubation, the non-adhesive cells were removed with the original culture medium and washed with fresh culture medium for 3 times. To promote proliferations, r-BMSCs on microspheres were transferred to the 6-well TCPs coated with sterile agarose from 48-well TCP, so as to obtain more space and more culture medium for cell growth. The culture medium was replaced every 48 h.

In brief, the scaffolds were washed three times with PBS and subsequently immersed in 2 μM fluorescein diacetate (FDA) and PI for 30 min at 37 °C. Fluorescence images were captured with a confocal laser scanning microscope (Nikon, Ti2, Japan), where live/dead cells display green/red fluorescence.

PicoGreen dsDNA Assay

DNA content to determine r-BMSCs proliferation, cellular DNA content was assessed using the Quant-It PicoGreen dsDNA assay (Thermo) following the instructions.

Cytoskeleton Staining

To conduct in situ observation, microspheres loaded with cells were fixed using 4% paraformaldehyde solution (Servicebio, China) for 20 min at room temperature and then washed three times with phosphate buffer saline (PBS). Subsequently, cells were immersed in 0.25% Triton X-100 solution for 20 min and then washed 3 times with PBS. To stain actin, cells were incubated with Phalloidin-Alex568 (Invitrogen, USA) for 40 min at room temperature and removed residual reagents with PBS to reduce the noisy backgrounds. Finally, stained cells on microspheres were observed under confocal laser scanning microscopy (CLSM, Nikon, Ti2, Japan).

Scanning Electron Microscopy

After fluorescence observation, microspheres loaded with cells were fixed for 10 h with 4% paraformaldehyde overnight and then dehydrated in ethanol solution with a series of concentrations of 30%, 50%, 60%, 70%, 80%, 90%, 95% and 100%, each for 15 min, respectively. They were subsequently treated under frozen drying overnight to remove residual ethanol for observation under scanning electron microscopy (SEM). 15s gold spaying was completed onto mold-made samples, followed by scanning at 5 kV.

In vitro Differentiation and Characterization

The r-BMSCs were seeded on microspheres, cultivated for 7 days and induced in osteogenic induction medium for 21 days. The osteogenic induction medium was added to replace the original medium. Osteo-inductive medium was exchanged at 2 day intervals. Using an alizarin red staining kit (Beyotime, China), calcium deposition (Ca) of cells on microspheres was observed under an optical microscope. Calcium content measurement: Mineralized samples were dissolved into 0.5 M acetic acid (0.4 mL) overnight and quantified by the calcium assay kit in line with specific protocols. To investigate osteogenesis-differentiation of r-BMSCs on/in microspheres, the expression levels of osteogenic genes on day 14 and day 21were estimated by quantitative real-time polymerization chain reaction analysis (qPCR). Four types of gene markers were found expressed, including bone morphogenetic protein 2 (BMP2), Osteocalcin (OCN), mothers against DPP homolog 1 (Smad1), and Runt-related transcription factor 2 (Runx2). The qPCR primers are listed in Table 1.

Table 1 Primers Used in qPCR

Primer name	Orientation	Sequence (5′-3′)
GAPDH	Forward	CCGAGGGCCCCACTAAAGG
	Reverse	TGCTGTTGAAGTCACAGGAGACA
RUNX2	Forward	AGATGATGACACTGCCACCTCTG
	Reverse	GGGATGAAATGCTTGGGAACT
BMP-2	Forward	CCACTCCACAAACGAGAAAAGC
	Reverse	CGCTTTTGCAGCTGGACTTAA
Smad-1	Forward	TTACCTGCCTCCTGAAGACC
	Reverse	TTCCGCATACACCTCTC
OCN	Forward	TGCCAGGTCACCAAATACCA
	Reverse	TGAGTACTGAGAGGCCCCAA

Rat Cranial Defects Model and in vivo Microcarriers Implantation

For evaluating whether microcarriers implant enhanced osteogenesis in vivo, this work utilized 40 male adult Sprague Dawley rats weighing 180–220 g and randomized them into 4 groups, including (i) Blank; (ii) PHA; and (iii) PHA-3% NP; (IV) PHA@r-BMSCs; (V) PHA-3%NP@BMSC (n = 10 rats per group). All surgical process in the experiments were approved by the animal ethics committee of Tongji Medical College, Huazhong University of Science & Technology (Wuhan, China). Sacrifice of animals was consistent with state regulations and laws and in accordance with the Standing Committee on Ethics in China (State Scientific and Technological Commission of China). The protocol was approved by the ethical committee (approval number: 2019-S1154). Preoperatively, isoflurane and subcutaneous injection of buprenorphine were used for rat anesthesia before making a 3-cm sagittal incision in the scalp center. The 5.0-mm diameter trephine was used to drill two parallel cranial defects in every rat, followed by implanting microspheres in the defect area and incision closure.

Micro-CT Analysis

At 4 and 12 weeks after surgery, rats were sacrificed to dissect the skulls, which were immersed within 4% paraformaldehyde. Micro-CT scanning was then conducted to assess bone tissues within defect areas (5 mm diameter). VG studio software was used to reconstruct sample 3D images.

Histological and Immunohistochemical (IHC) Analyses

All samples were formalin-fixed for 7 days and subsequently decalcified in EDTA for 1 month followed by paraffin embedding, dehydration with gradient ethanol and slicing in 3-μm sections for hematoxylin and eosin (H&E, Beyotime, China) and Masson's trichrome staining. The antibodies are listed in Table 2. Histological and immunohistochemical images were recorded.

Table 2 Antibodies

Antibody Name	Dilution	Company	Cat.no.
Anti-OCN	1:100	Abcam	ab93876
Anti-Col1	1:200	Abcam	ab6308
Phalloidin	1:1000	Abcam	ab176757

Statistical Analysis

All data are shown as the mean ± standard deviation. Each assay had at least three replicates and was repeated three times independently. One-way analysis of variance (ANOVA) or two-way ANOVA followed by Tukey, Sidak, or Bonferroni correction or the two-tailed Student's *t*-test was performed to analyze the statistical significance. Statistical significance was set at $P < 0.05$.

Results

Preparation and Characterization of Microspheres

Morphology and Nile red staining of PLA, PCL, and PHA microspheres reveal that the pore walls of the PLA, PCL, and PHA solid microspheres (SMs) are smooth (Figure 1A). Conversely, PLA, PCL, and PHA OPMs have a large surface area with pores throughout the OPMs (Figure 1B). Confocal laser microscopy (CLSM) was used to evaluate the viability and distribution of r-BMSCs cultured on the microspheres on days 1, 5, and 10 after cell seeding. Representative images of PLA, PCL, and PHA solid microspheres and porous microspheres by live-dead cell staining were revealed (Figure 1A and B). The average number of r-BMSCs on the solid microspheres began to reduce but r-BMSCs on the porous microspheres continued to proliferate from day 1 to day 10. R-BMSCs proliferated well on open porous PLA, PCL, and PHA microspheres compared to the r-BMSCs on solid microspheres. The largest amount of r-BMSCs proliferated and migrated on PHA OPMs (Figure 1C and D). Cytoskeleton staining images of r-BMSCs proliferated on PLA, PCL, and PHA OPMs and SMs showed that more cells proliferated on the PHA OPMs than other microspheres on day 10, which was consistent with the live-dead cell staining (Figure 1E and F).

Preparation and Characterization of Composite PHA-NP OPMs

PHA-NP microspheres were prepared using the gas-liquid double emulsion (Figure 2A). PHA-NP OPMs diameters ranged from 100 to 800 μm, with a highly open and interconnected porous surface (Figure S1A and B). The overall porosity rate of the microspheres decreased as the NP concentrations increased, with higher porosity rate at NP concentrations of 1–3% (Figure 2B). The results indicated that NP-based scaffold integrity rate also decreased as NP concentration increased, with higher integrity rate at NP concentrations of 1–3% (Figure S1C). Fourier Transform Infrared Spectroscopy (FTIR) was employed to verify the obtained microsphere compositions. All samples exhibit the characteristic peaks of PHA. The characteristic peaks of nano-clay were found in PHA-1%NP, PHA-3%, and PHA-5% (Figure S1D).

PHA-3% NP porous microspheres with NP critical concentration were selected for further microsphere preparation parameter studies. The microsphere porosity changed significantly as primary emulsification stirring speeds increased from 8,000,10,000 to 12,000 rpm (Figure 2C). Compared to PHA-3%NP OPMs produced by 8,000 rpm primary emulsification stirring speeds, the porosity of PHA-3%NP OPMs produced by 10,000 rpm and 12,000 rpm primary emulsification stirring speeds decreased to approximately 15% and 11%, respectively (Figure 2D). However, the microsphere morphology and porosity did not change significantly as secondary emulsification stirring speeds increased from 200, 400, to 600 rpm (Figure 2E and F). Figure 2G and H depicted that as the diameter of porous microspheres increased from 100 to 300 μm, their porosity gradually increased (Figure 2G and H). Cytoskeleton staining images showed that the largest amount of r-BMSCs proliferated and migrated on 300μm PHA −3% NP OPMs from day 4 to 14 (Figure 2I and J). Therefore, microspheres with a primary emulsification rate of 8,000 rpm, a secondary emulsification rate of 400 rpm and a diameter of 300 μm were chosen for further research.

In vitro r-BMSC Encapsulation

Bright field images of microspheres show similar surface morphology of PHA microspheres with different NP concentrations at 300 μm size (Figure 3A). The biocompatibility of microspheres was evaluated using r-BMSC culture and viability tests. CLSM was used to evaluate the viability and distribution of r-BMSCs cultured on the microspheres on days 1, 4, 7, and 10 after cell seeding. Bright green fluorescence reveals that the cells are healthy, with red signal strands for dead cells (Figure 3B). No obvious toxicity was found on all these microspheres, and cell viability was higher at the

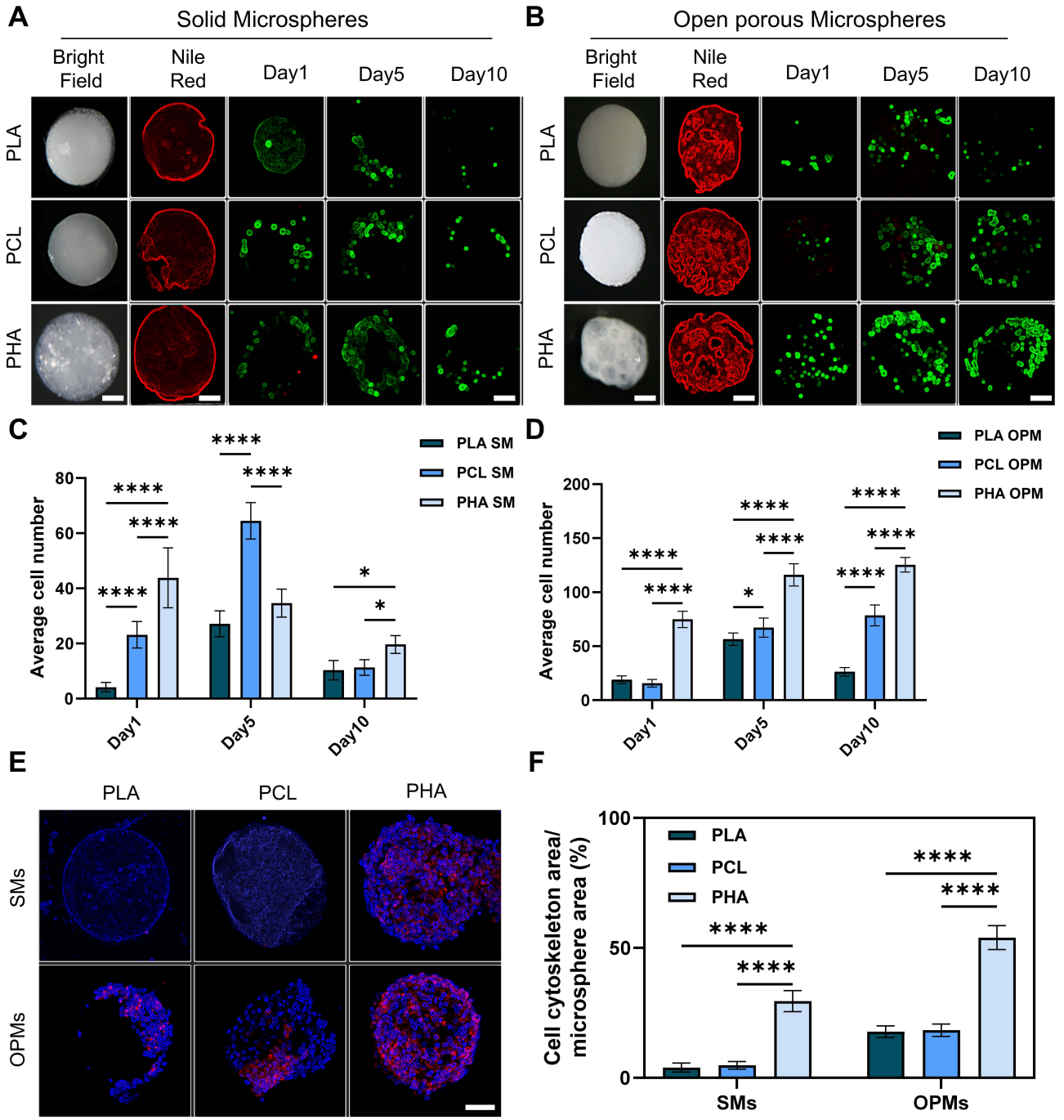

Figure 1 Preparation, morphology, and biocompatibility of PLA, PCL, and PHA OPMs and SMs. (**A**) Morphology, Nile red staining and live and dead r-BMSCs of PLA, PCL, and PHA SMs. (**B**) Morphology, Nile red staining and live and dead r-BMSCs of PLA, PCL, and PHA OPMs. (**C**) Quantification of average cell number on PLA, PCL, and PHA SMs from days 1 to 10. (**D**) Quantification of average cell number on PLA, PCL, and PHA OPMs from days 1 to 10. (**E**) CLSM images of r-BMSCs cultured on the PLA, PCL, and PHA OPMs and SMs with phalloidin on days 10 (red: β-actin, blue: 4',6-diamidino-2-phenylindole (DAPI)). (**F**) Quantification of r-BMSCs cytoskeleton area/microsphere area of PLA, PCL, and PHA OPMs and SMs on days 10. The bars are 100 μm. (*p < 0.05; ****p < 0.0001).

later time points when NP was incorporated (Figure 3B and C). The viability of r-BMSCs grown on the PHA-3%NP microspheres was higher than any other group from day 1 to day 10. (Figure 3B and C). Figure 3D depicts cell proliferation from days 1 to 14, with the microspheres covered with a red fluorescence-stained cytoskeleton. Cells can adhere with extended filopodia to all microspheres. However, the r-BMSCs spread more extensively on the PHA-3%NP than on others (Figure 3E). When the culture period was extended to 14 days, a significantly higher growth rate was

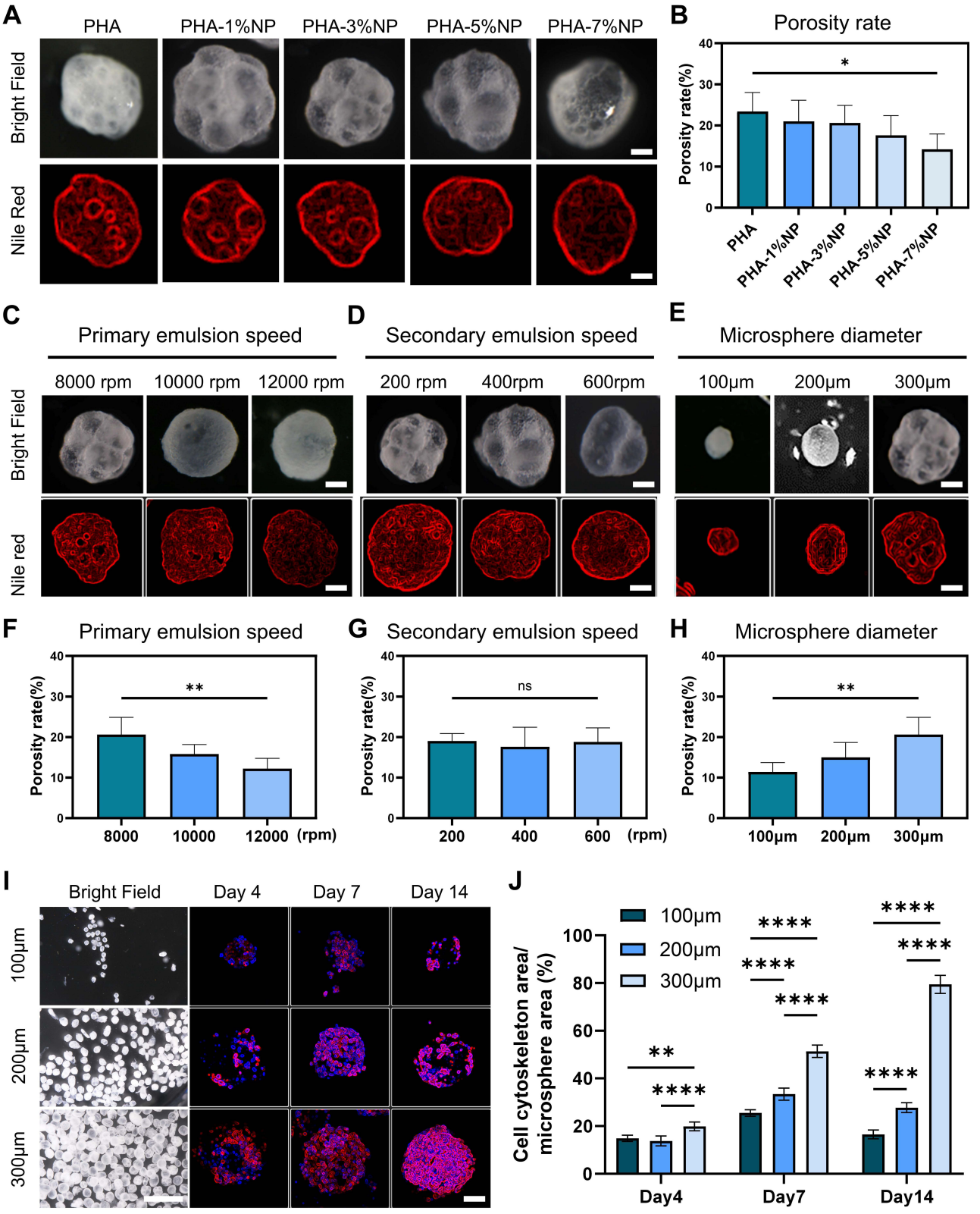

Figure 2 Fabrication and optimization of PHA OPMs and PHA-NP OPMs. (**A**) Morphology and Nile red staining of PHA OPMs and PHA-NP OPMs. (**B**) Porosity rate of PHA OPMs and PHA-NP OPMs. (**C**) Morphology and Nile red staining of PHA-3%NP OPMs with different homogenizer speeds during primary emulsification. (**D**) Porosity rate of PHA-3%NP OPMs with different homogenizer speeds during primary emulsification. (**E**) Morphology and Nile red staining of PHA-3%NP OPMs with different homogenizer speeds during secondary emulsification. (**F**) Porosity rate of PHA-3%NP OPMs with different homogenizer speeds during secondary emulsification. (**G**) Morphology and Nile red staining of PHA-3%NP OPMs with different size. (**H**)Porosity rate of PHA-3%NP OPMs with different size. (**I**) Phalloidin CLSM images of r-BMSCs cultured on PHA-3%NP OPMs with different size from days 4, 7, and 14 (red: β-actin, blue: DAPI). (**J**) Quantification of r-BMSCs cytoskeleton area/microsphere area on PHA-3%NP OPMs with different size on days 4, 7, and 14. Data for each sample were obtained from > 200 parallels randomly selected from 20 microspheres. The bars are 100 μm. (*p < 0.05; **p < 0.01; ****p < 0.0001).

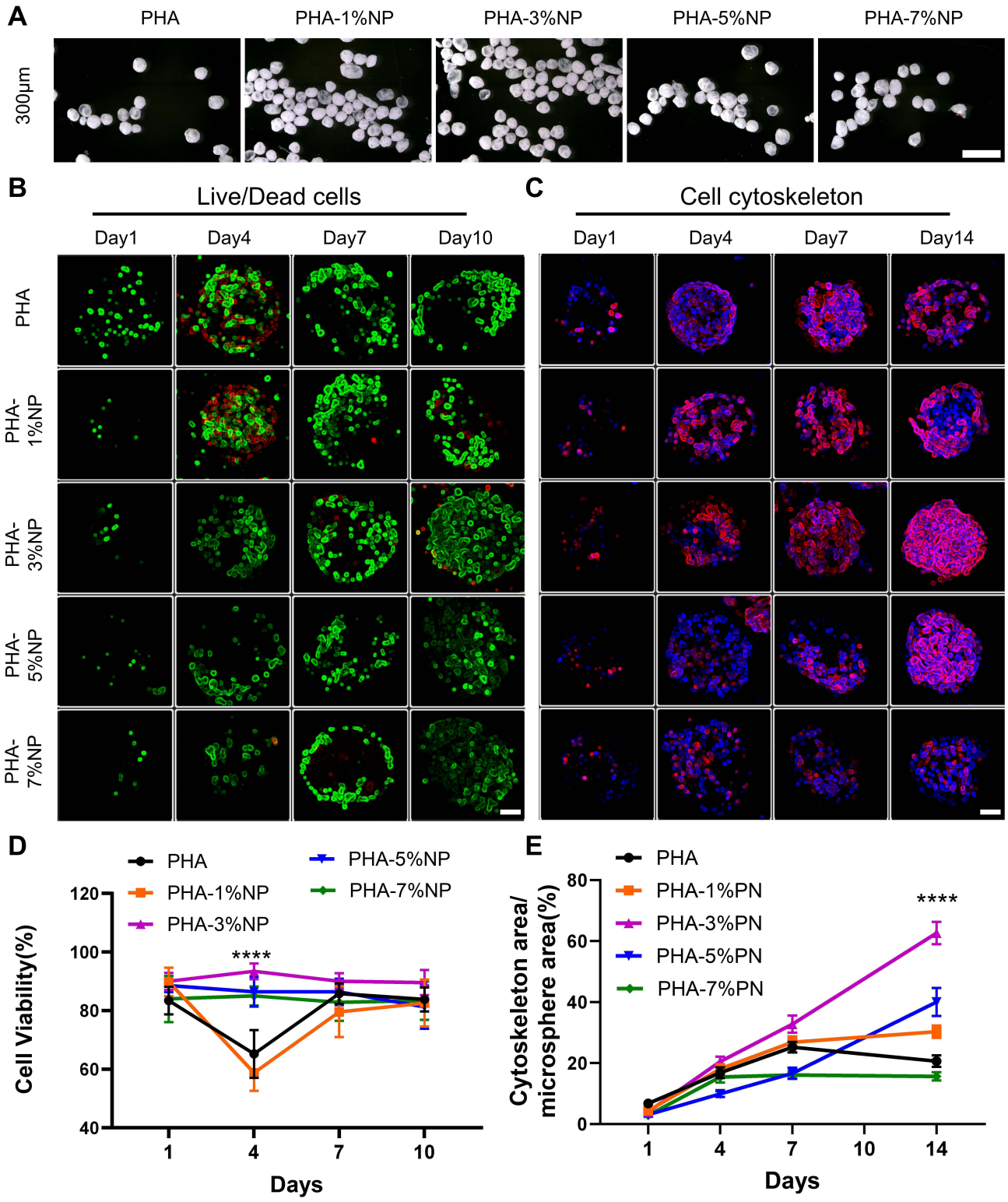

Figure 3 Proliferation of r-BMSCs on/in PHA OPMs and PHA-NP OPMs. (**A**) Bright field images of PHA OPMs and PHA-NP OPMs with 300μm size. The bars are 1mm. (**B**) CLSM images of r-BMSCs cultured on the microspheres with live/dead cell staining on days 1, 4, 7, and 10 (green: live cells, red: dead cells, blue: DAPI). The bars are 100 μm. (**C**) Quantitative analysis revealed cell viability on the OPMs on days 1, 4, 7, and 14. (**D**) CLSM images of r-BMSCs cultured on the microspheres with phalloidin on days 1, 4, 7, and 14 (red: β-actin, blue: DAPI). The bars are 100 μm. (**E**) Quantitative analysis revealed the cytoskeleton area/microsphere area on the OPMs on days 1, 4, 7, and 14. (****$p < 0.0001$).

observed in the PHA-3%NP group, as indicated by the calculated result of cells in the scaffolds (Figure 3E). Cell growth on the PHA-3%NP scaffold was more promising than that on the other PHA-NP scaffold, possibly due to the higher NP concentration in the PHA-NP scaffold, which promoted cell growth. The PHA-3%NP scaffold with a primary emulsification rate of 8,000 rpm, secondary emulsification rate of 400 rpm and diameter of 300 μm were chosen as the microspheres to repair cranial defects and load more cells based on the above findings.

In vitro Osteogenesis of r-BMSCs Cultured on Microspheres

Both PHA-3%NP and PHA microspheres have homogeneous pores on the surface and inside the microsphere. Additionally, r-BMSCs could adhere to the beam and steadily proliferate as the culture time increased. The adhesion and growth state of r-BMSCs on microspheres were comprehensively examined using SEM. R-BMSCs spread well on external frameworks and inner microspheres (Figure 4A). Compared to PHA microspheres, the higher number of pores on/in the PHA-3%NP microspheres may be more beneficial for cell proliferation (Figure S1E, F and 4B). The Cell Counting Kit-8 assay was used to assess cell proliferation in the scaffolds on days 1, 4, 7, and 10. As anticipated, all scaffolds exhibited non-significant toxicity after 10 days of co-culturing. The proliferation rate was higher in the PHA-3%NP OPMs group than in PHA OPMs after 10 days (Figure 4C). Figure 4D depicts the Pico Green dsDNA assay data correlating to cellularity. DNA content in the NP-containing microspheres increased gradually, revealing significant improvements over the non-NP-containing PHA microsphere counterparts after 10 days (Figure 4D).

Bone-related genes, including bone morphogenetic protein 2 (BMP2), Osteocalcin (OCN), mothers against DPP homolog 1 (Smad1), and Runt-related transcription factor 2 (Runx2), respectively, were observed up-regulated for cells on/in PHA-3%NP@BMSC group, whereas these gene expressions in cells on PHA microspheres showed only a slight increase or no change on 21d (Figure 4E–H).

R-BMSCs on/in OPMs can be induced in vitro to osteogenesis. After 7 d of proliferation, r-BMSCs on/in microspheres were transferred to osteogenic induction medium (OIM) and incubated for 21 days. On day 14 and day 21, alizarin red staining, an osteogenesis marker of calcium nodules, was found to be significantly higher on/in PHA-3%NP OPMs than that detected PHA OPMs. Furthermore, increased calcium depositions (Ca) observed under alizarin red staining were visible with PHA-3%NP OPMs from day 14 to day 21 (Figure 4I). High calcium deposition for cells on PHA-3%NO OPMs can be attributed to improved mechanical properties by the NP (Figure 4J).

In vivo Application of Cell Loaded Composite Microspheres in Bone Regeneration

Micro-CT Evaluation

As PHA-3%NP@BMSC scaffolds showed in vitro osteogenesis, further analysis of in vivo osteogenic effect was conducted in rat cranial defect models (5mm in diameter) (Figure S2A). Rat euthanasia was performed at 4 and 12 weeks postoperatively. Then, the defect locations were gathered, aiming to evaluate bone repair through micro-CT analysis and histology (Figure 5A).

Micro-CT was used to reveal the new bones generated in bone defects at 4 weeks and 12 weeks post-implantation. A small amount of newly formed bone was observed in 3D reconstruction images after 4 weeks of treatment. When the treatment period was prolonged to 12 weeks, PHA-3%NP@BMSC group exhibited more newly formed bone tissue than the other groups in 3D reconstruction images (Figure 5B). Finally, micro-CT showed that PHA-3%NP@BMSC group had more than 2-fold higher bone volume (Figure 5C), bone volume/total volume ratio (Figure 5D) than NC and PHA microsphere group.

Histological Analysis of Bone Regeneration

Hematoxylin and eosin staining (Figure 5E and F) and Masson's trichrome staining (Figure 6A) of the scaffolds revealed PHA-3%NP@r-BMSC microspheres exhibit slow degradation rates compared to pure PHA microspheres. There were only a few new bones formed in the control group. On the contrary, a large number of osseous tissues along the junction of the defects were observed in the PHA-3%NP@r-BMSCs group at 12 weeks. This was consistent with the micro-CT observation that the nano-clay could promote bone healing in vivo. Consistent with H & E staining, Masson's trichrome staining revealed that consecutive collagen fiber bundles and ossified tissues were arranged compactly in the defect area

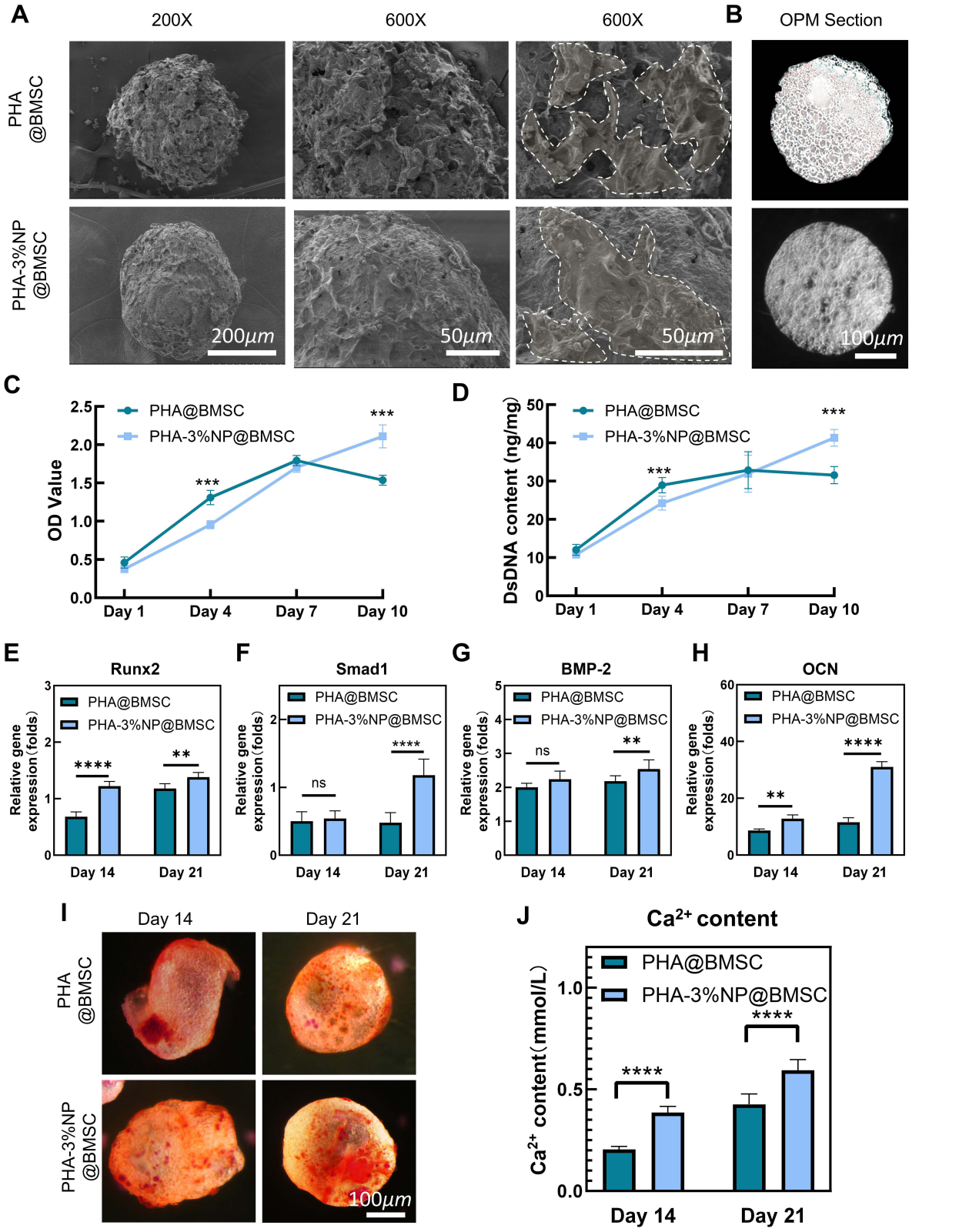

Figure 4 Morphology and in vitro differentiation of r-BMSCs on/in OPMs (**A**) SEM images of r-BMSCs grown on the PHA OPMs and PHA-3%NP OPMs. (**B**) Bright field images of section of PHA OPMs and PHA-3%NP OPMs. (**C**) CCK-8 analysis of r-BMSCs on/in PHA OPMs, PHA-3%NP OPMs on days 1, 4, 7, and 10. (**D**) Pico Green dsDNA assay of r-BMSCs on/in PHA OPMs, PHA-3%NP OPMs on days 1, 4, 7, and 10. (**E-H**) Quantitative real-time polymerization chain reaction of bone-related gene markers expression of r-BMSCs during osteo-inductive differentiation for 14 and 21 days on/in PHA OPMs versus PHA-3%NP OPMs. (**I**) Alizarin red staining of calcium (Ca^{2+}) deposition of r-BMSCs grown on/in microspheres. The bars are 100 μm. (**J**) Quantitative analysis of Ca^{2+} deposition of r-BMSCs grown on/in microspheres. (**p < 0.01; ***p < 0.001; ****p < 0.0001).

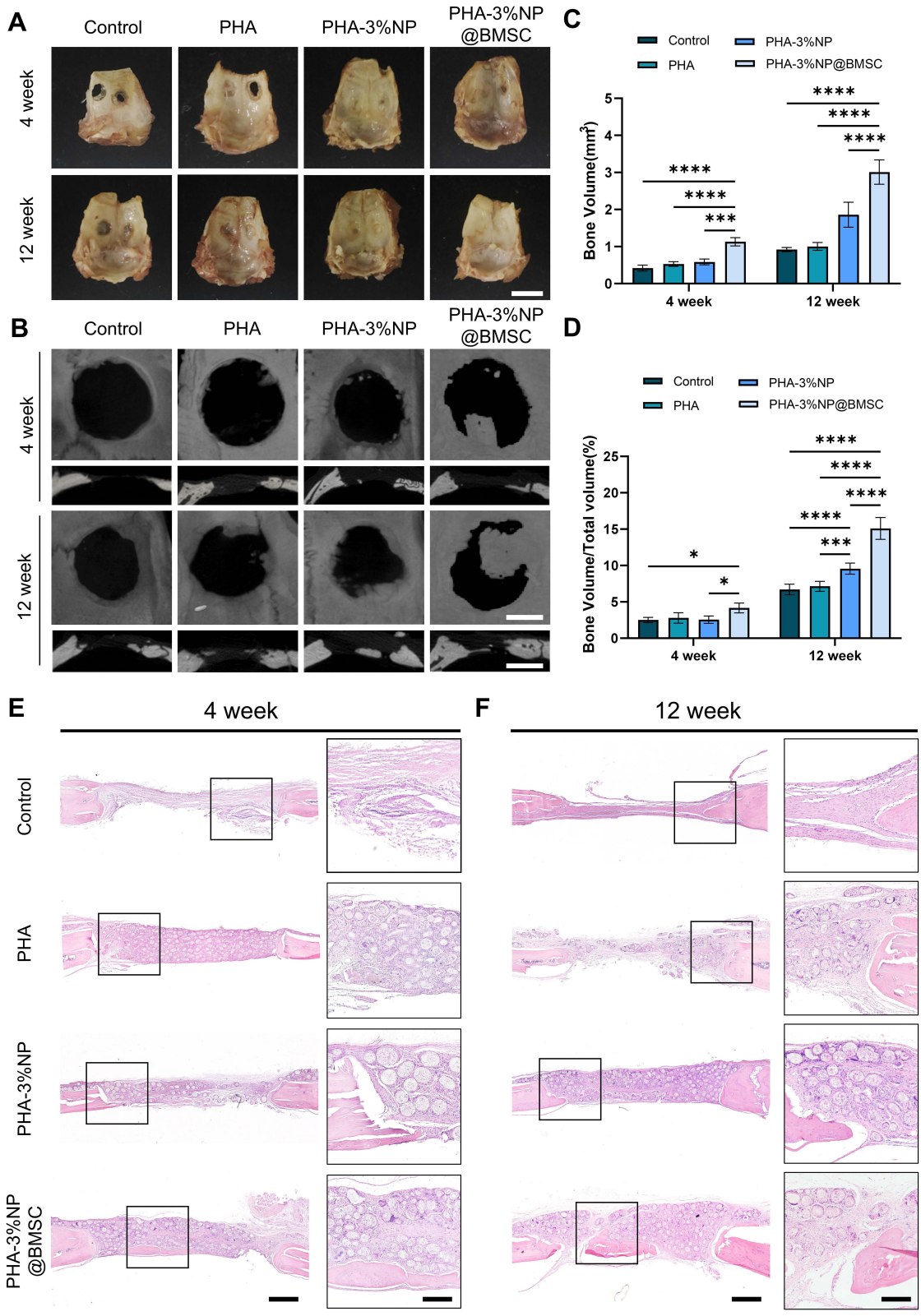

Figure 5 In vivo evaluation of new bone formation. (**A**)Macroscopic observation of implantation samples 4 and 12 weeks after surgery. The bars are 1cm. (**B**) Micro-CT 3D reconstruction images showing bone defects at 4 and 12 weeks after implantation. The bars are 2.5 mm. (**C**)Quantitative analysis of the micro-CT data of Bone volume and (**D**) bone volume/total volume ratio of porous microspheres. (**E**) Images of H&E staining of cranial defects recovery at 4 weeks after implantation. (**F**) Images of H&E staining of cranial defects recovery at 12 weeks after implantation. The bars are 1mm. (*p < 0.05; ***p < 0.001; ****p < 0.0001).

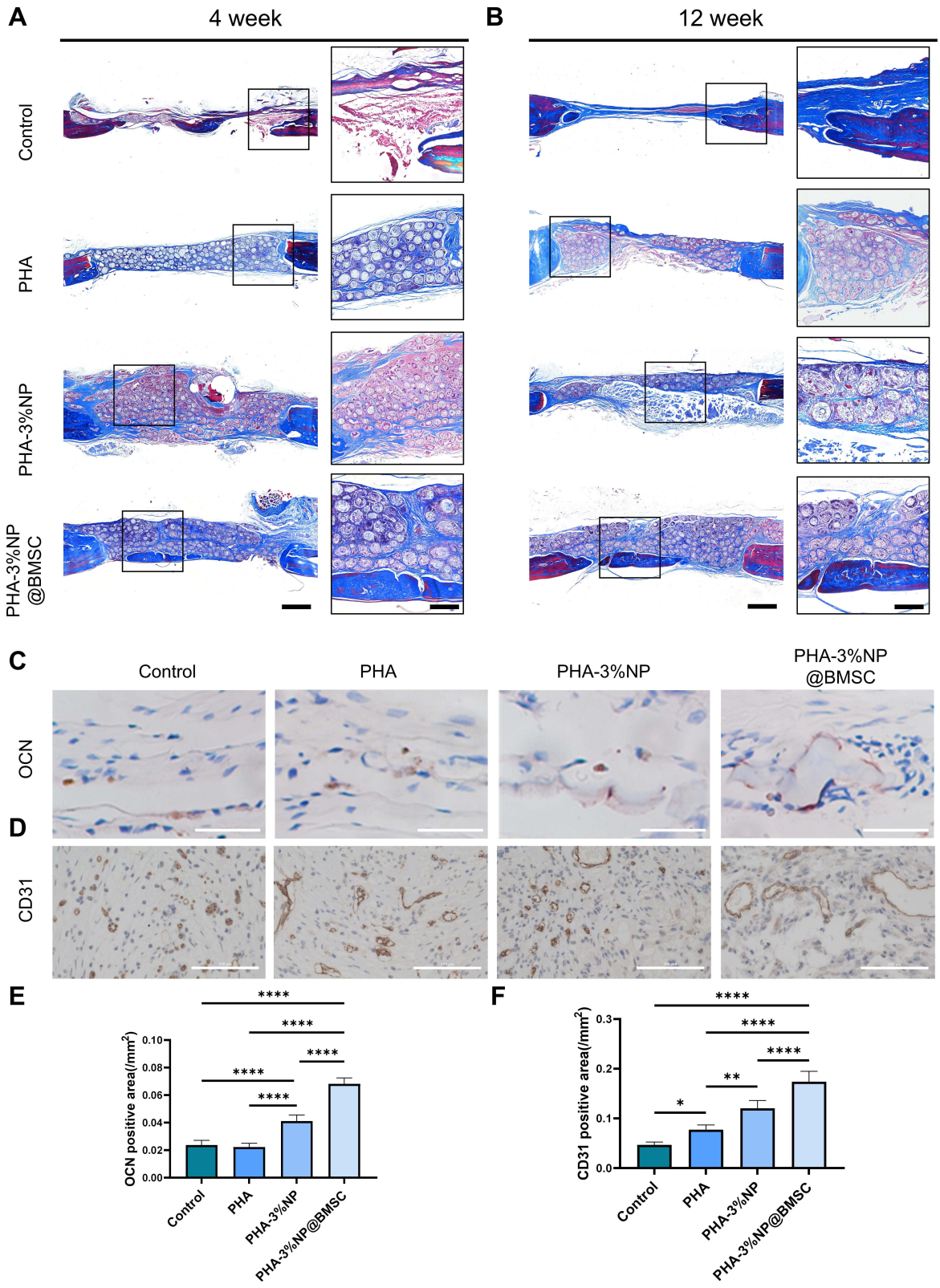

Figure 6 Histological and immunohistochemical analysis following scaffolds implantation. (**A**) Images of Masson's trichrome staining of cranial defects at 4 weeks after implantation. (**B**) Images of Masson's trichrome staining of cranial defects at 12 weeks after implantation. The bars are 1mm. (**C**) IHC analysis of OCN at 12 weeks following scaffold implantation. The bars are 100μm. (**D**)IHC analysis of CD31 at 12 weeks following scaffold implantation. The bars are 100μm. (**E**)Quantitative analysis of OCN at 12 weeks following scaffold implantation. (**F**) Quantitative analysis of CD31 at 12 weeks following scaffold implantation. (*p < 0.05; **p < 0.01; ****p < 0.0001).

in the PHA-3%NP@r-BMSCs group, while the control groups only demonstrated the connected fibers with a few new bones formed (Figure 6A and B). The other groups presented the behaviors in between the PHA-3%NP@r-BMSC and control groups. The results of the osteogenesis efficiency were further confirmed by immunohistochemical staining of OCN, which was expressed to the highest extent in PHA-3%NP@r-BMSC group as well. In order to evaluate neovascularization in the bone defect area, the CD31 immunohistochemical staining was further performed. Immunohistochemistry analysis revealed that the PHA-3%NP@BMSCs group exhibited the largest CD31 positively expressed area. The quantitative analysis of the number of vessels further confirmed the observed results (Figure 6C–F).

Discussion

Cranial defect is common sequela after injury and surgery, affecting millions of patients globally.[2,7,42] The incidence of cranial defect syndrome and secondary brain injury is high, making timely skull repair crucial.[2,7] There is a wide range of cranial defect repair materials available, yet the current options still fail to fully meet clinical needs.[6,19] Autogenous bone graft is prone to absorption, difficult to preserve, and susceptible to infection. Silicone rubber materials, with their electrostatic surfaces, easily attract foreign bodies, leading to postoperative foreign body reactions. Metallic materials (such as titanium mesh) conduct heat and electricity, potentially causing chronic brain tissue damage due to temperature fluctuations.[6,8,34,36] Inappropriate selection of skull repair materials or unsatisfactory shaping can result in surgical failure, increased susceptibility to infection, and even death in severe cases.[5,33,34] Therefore, the development of new skull repair strategies holds significant importance.

PHA-3%NP@r-BMSCs with osteo-inductivity, biodegradability, and high specific surface area have the potential to be developed as biomaterial scaffolds for filling bone defects as they can effectively promote the vascularization and osteogenesis in the bone defect regenerated microenvironment, thereby improving the quality of bone repair. The important foundation for tissue engineering repair of cranial defects lies in good biocompatibility, appropriate hardness, and osteo-conductivity biomaterials.[43] Composite made from natural polymers PHA and NP are promising candidates for enhancing bone regeneration by mimicking the compositions of native bone.[16,34] This material stiffness was intended to facilitate r-BMSCs differentiation into osteoblasts. Compared to common biopolymers such as PLA and PLGA, the most prominent feature of PHA is that its biodegradation does not lead to the rapid release of lactic acid or glycolic acid, which can be harmful to cells and tissues.[11,19,22,23]

Nano-clays demonstrate good osteo-conductivity, meaning they can guide the growth and differentiation of bone cells on their surface, thereby accelerating the regeneration process of bone tissue.[34] This pro-osteoblastic activity of NP may be due to nontoxic degradation products, such as Li, Si(OH) 4, and Mg2+, and the interactions with cellular components.[34] Nano-clays can also be combined with other bioactive molecules or nanomaterials to form composites with multiple functions. For example, by combining nano-clays with organic hydrogels, bone sealants with self-healing, antibacterial, and antioxidant activities can be prepared.[44,45] However, the strength of this composite material is insufficient to support the repair of cranial defects. PHA-NP materials exhibit good biocompatibility, enabling them to form stable interfaces with surrounding tissues in vivo, reducing the occurrence of rejection reactions and inflammatory responses.

Porous microspheres, compared to traditional bulk biomaterials, possess a larger specific surface area, which facilitates accelerated transfer rates of oxygen and nutrients.[40,46] This characteristic significantly enhances the efficiency of cell loading on the surface of the microspheres, while also better maintaining the differentiation phenotype of the cells. This provides a more favorable microenvironment for the repair of cranial defects.[18,19] PHA-NP microspheres, which preserve the open porous structure, are excellent injectable micro-scaffolds for tissue engineering. The porous structure of PHA-3%NP@r-BMSCs aids in cell-to-cell connections and communication, further promoting cell proliferation and differentiation. When applied in vivo, PHA-3%NP porous microspheres provide a 3D biomimetic microenvironment similar to that in vivo. Nano-clay exhibits good osteogenic capacity, promoting the proliferation and differentiation of loaded r-BMSCs on the scaffold, thereby facilitating the repair of cranial defects (Figure 5E and F, 6A and B). In the future, with the continuous development of nanotechnology and biotechnology, the application prospects of PHA-3% NP@r-BMSCs in bone repair will become even broader.

The joint effect of the r-BMSCs and nano-clay is more clearly observed during histological examination for tissue response and integration. The combined effect of r-BMSCs and nano-clay can improve the osteo-conductivity and osteo-inductivity of synthetic PHA microspheres for enhanced bone formation and scaffold integration (Figure 6A and B). Previous studies required the incorporation of mineral content or osteogenic growth factors to induce bone tissue infiltration in the rat cranial defect.[18] The positive endogenous regenerative outcome of PHA-3%NP@BMSCs could be due to bone-enhancing nano-clay and several r-BMSC paracrine effects, including the secretion of factors that recruit host cells.

The degradation mode of most PHAs is unique and mild, with PHA undergoing gradual degradation over a period of approximately 1 to 5 years.[24,28,29] The non-toxic degradation products can be gradually absorbed by the body. PHA degradation rates reported in both in vivo and in vitro studies in the literature may provide some reference value for this research. According to limited literature reports, the fiber membranes prepared from P34HB degrade by 6.2 ± 0.72% in vitro within the first month and by 12.2 ± 0.41% in vitro within the second month.[25] In addition, degradation rates of P34HB not only relevant to in vivo or in vitro degradation microenvironment but also associated with morphologies, grafting ratios, and molecular weights, as reported in the literature.[26–28] We hope this information can provide some reference for our study.

PHA-3%NP@BMSC microspheres exhibit slow degradation rates, which may facilitate the maintenance of the morphology for an extended period in vivo (Figure 6A and B). We observed that by the fourth week, neovascularization and abundant immune cells had begun to appear around the PHA-3%NP@BMSC. As the cranial bone gradually repairs, PHA-3%NP@BMSC gradually degrades in rats. By the twelfth week, the morphology of the microspheres began to change, transitioning from round to oblate, and more blood vessels started to grow into them. P34HB is a biomaterial with excellent biocompatibility and biodegradability, and it can be developed into microspheres loaded with BMSCs for cranial bone repair. Neo-bone tissue has grown into a porous structure, tightly integrating the micro-scaffold with the surrounding tissue. The degradation rate and structural stability of the micro scaffold must be consistent with the ossification rhythm.

PHA-3%NP@BMSC microspheres exhibit low swelling and slow degradation rates, making them suitable for cranial defect repair. Experimental validation has confirmed their excellent repair effects. To more intuitively observe the degradation rate of PHA-3%NP@BMSC in vivo, we plan to utilize PHA-3%NP@BMSC for long-term cranial bone repair in large animals, such as pigs or monkeys, which will enable us to observe the degradation rate in vivo on an annual basis. Lastly, but importantly, additional studies are required to elucidate the specific mechanisms and detailed pathways through which PHA-3%NP@BMSC promotes the repair of cranial defects.

Conclusion

PHA-3%NP@r-BMSCs with osteo-inductivity, biodegradability, and high specific surface area have the potential to be developed as biomaterial scaffolds for filling bone defects as they can effectively promote the vascularization and osteogenesis in the bone defect regenerated microenvironment, thereby improving the quality of bone repair.

Acknowledgments

This work was supported by the National Natural Science Foundation of China (No. 82322046, 82020108020, 82072198, 81873941, 81701922, 32201111), the National Key R&D Program of China (2019YFA0110500), the Key Science and Technology Project of Guangzhou City (No.2023B03J1231), the Science and Technology Project Plan of Shihezi University(ZZZC2022093), the Open Foundation of Hubei Key Laboratoryof Regenerative Medicine and Multi-disciplinary Translational Research(2024zsyx08) and 2024KQHM02.

Disclosure

The authors report no conflicts of interest in this work.

References

1. Hassanein AH, Arany PR, Couto RA, et al. Cranial particulate bone graft ossifies calvarial defects by osteogenesis. *Plast Reconstr Surg*. 2012;129(5):796–802. doi:10.1097/PRS.0b013e31824a2bdd
2. Li Y, Zha Y, Hu W, et al. Monoporous microsphere as a dynamically movable drug carrier for osteoporotic bone remodeling. *Adv Healthc Mater*. 2023;12(16):1–12. doi:10.1002/adhm.202201242
3. Li Y, Zhang X, Dai C, et al. Bioactive three-dimensional graphene oxide foam/polydimethylsiloxane/zinc silicate Scaffolds with enhanced osteoinductivity for bone regeneration. *ACS Biomater Sci Eng*. 2020;6(5):3015–3025. doi:10.1021/acsbiomaterials.9b01931
4. Dai C, Li Y, Pan W, et al. Three-dimensional high-porosity Chitosan/Honeycomb Porous Carbon/Hydroxyapatite Scaffold with enhanced osteoinductivity for bone regeneration. *ACS Biomater Sci Eng*. 2020;6(1):575–586. doi:10.1021/acsbiomaterials.9b01381
5. Guo L, Chen H, Li Y, Zhou J, Chen J. Biocompatible scaffolds constructed by chondroitin sulfate microspheres conjugated 3D-printed frameworks for bone repair. *Carbohydr Polym*. 2023;299(September 2022):120188. doi:10.1016/j.carbpol.2022.120188
6. Miljanovic D, Seyedmahmoudian M, Stojcevski A, Horan B. Design and fabrication of implants for mandibular and craniofacial defects using different medical-additive manufacturing technologies: a review. *Ann Biomed Eng*. 2020;48(9):2285–2300. doi:10.1007/s10439-020-02567-0
7. Wang Y, Li W, Guo Y, et al. Mitochondria transplantation to bone marrow stromal cells promotes angiogenesis during bone repair. *Adv Sci*. 2024. doi:10.1002/advs.202403201
8. Hoffmann KJ, Büsch C, Moratin J, Ristow O, Hoffmann J, Mertens C. Peri-implant health after microvascular head and neck reconstruction—A retrospective analysis. *Clin Oral Implants Res*. 2024;35(2):187–200. doi:10.1111/clr.14214
9. Wang W, Xiong Y, Zhao R, Li X, Jia W. A novel hierarchical biofunctionalized 3D-printed porous Ti6Al4V scaffold with enhanced osteoporotic osseointegration through osteoimmunomodulation. *J Nanobiotechnol*. 2022;20(1):1–19. doi:10.1186/s12951-022-01277-0
10. Wu L, Gu Y, Liu L, et al. Hierarchical micro/nanofibrous membranes of sustained releasing VEGF for periosteal regeneration. *Biomaterials*. 2020;227(July 2019):119555. doi:10.1016/j.biomaterials.2019.119555
11. Yuan S, Shen Y, Li Z. Injectable cell- and growth factor-free poly(4-hydroxybutyrate) (P4HB) microspheres with open porous structures and great efficiency of promoting bone regeneration. *ACS Appl Bio Mater*. 2021;4(5):4432–4440. doi:10.1021/acsabm.1c00188
12. Gu X, Zha Y, Li Y, et al. Integrated polycaprolactone microsphere-based scaffolds with biomimetic hierarchy and tunable vascularization for osteochondral repair. *Acta Biomater*. 2022;141:190–197. doi:10.1016/j.actbio.2022.01.021
13. Wang Y, Yuan Z, Pang Y, et al. Injectable, high specific surface area cryogel microscaffolds integrated with osteoinductive bioceramic fibers for enhanced bone regeneration. *ACS Appl Mater Interfaces*. 2023;15(17):20661–20676. doi:10.1021/acsami.3c00192
14. Xia H, Wang L, Li C, et al. Synthesis of fully porous silica microspheres with high specific surface area for fast HPLC separation of intact proteins and digests of ovalbumin. *Microchim Acta*. 2020;187(7). doi:10.1007/s00604-020-04327-2
15. Zhang W, Wang XC, Li XY, Zhang L, Jiang F. A 3D porous microsphere with multistage structure and component based on bacterial cellulose and collagen for bone tissue engineering. *Carbohydr Polym*. 2020;236(November 2019):116043. doi:10.1016/j.carbpol.2020.116043
16. Yuan X, Yang W, Fu Y, et al. Four-arm polymer-guided formation of curcumin-loaded flower-like porous microspheres as injectable cell carriers for diabetic wound healing. *Adv Healthc Mater*. 2023;12(30):1–22. doi:10.1002/adhm.202301486
17. Yuan Z, Yuan X, Zhao Y, et al. Injectable GelMA cryogel microspheres for modularized cell delivery and potential vascularized bone regeneration. *Small*. 2021;17(11):1–13. doi:10.1002/smll.202006596
18. Han S, Yang H, Ni X, et al. Programmed release of vascular endothelial growth factor and exosome from injectable chitosan nanofibrous microsphere-based PLGA-PEG-PLGA hydrogel for enhanced bone regeneration. *Int J Biol Macromol*. 2023;253(P1):126721. doi:10.1016/j.ijbiomac.2023.126721
19. Hu X, Yang S, Zhao W, et al. Novel multi-functional microsphere scaffold with shape memory function for bone regeneration. *Biomater Adv*. 2024;163(July):213958. doi:10.1016/j.bioadv.2024.213958
20. Li X, Li X, Yang J, et al. Living and injectable porous hydrogel microsphere with paracrine activity for cartilage regeneration. *Small*. 2023;19(17):1–14. doi:10.1002/smll.202207211
21. Heo Y, Shin SW, Kim DS, et al. Bioactive PCL microspheres with enhanced biocompatibility and collagen production for functional hyaluronic acid dermal fillers. *Biomater Sci*. 2022;10(4):947–959. doi:10.1039/d1bm01846a
22. Hyodo N, Gan H, Ilangovan M, et al. Coastal and deep-sea biodegradation of polyhydroxyalkanoate microbeads. *Sci Rep*. 2024;14(1):1–11. doi:10.1038/s41598-024-60949-z
23. Rodríguez-Cendal AI, Gómez-Seoane I, de Toro-Santos FJ, Fuentes-Boquete IM, Señarís-Rodríguez J, Díaz-Prado SM. Biomedical applications of the biopolymer poly(3-hydroxybutyrate-co-3-hydroxyvalerate) (PHBV): drug Encapsulation and Scaffold Fabrication. *Int J Mol Sci*. 2023;24(14):11674. doi:10.3390/ijms241411674
24. Liu W, Jiao T, Su Y, et al. Electrospun porous poly(3-hydroxybutyrate- co −4-hydroxybutyrate)/lecithin scaffold for bone tissue engineering. *RSC Adv*. 2022;12(19):11913–11922. doi:10.1039/d2ra01398c
25. Lu T, Yang L, Li Z, Liu Y, Xu S, Ye C. Immediate implantation of ultrafine fiber slow-release system based on cell electrospinning to induce osteogenesis of mesenchymal stem cells. *Regen Biomater*. 2024;11(August 2023). doi:10.1093/rb/rbad113
26. Zhou T, Li G, Lin S, et al. Electrospun poly(3-hydroxybutyrate-co-4-hydroxybutyrate)/graphene oxide Scaffold: enhanced properties and promoted in vivo bone repair in rats. *ACS Appl Mater Interfaces*. 2017;9(49):42589–42600. doi:10.1021/acsami.7b14267
27. Gładysz MZ, Ubels D, Koch M, et al. Melt Electrowriting of Polyhydroxyalkanoates for Enzymatically Degradable Scaffolds. *Adv Healthc Mater*. 2024;2401504:1–15. doi:10.1002/adhm.202401504
28. Li J, Chen JN, Peng ZX, et al. Multifunctional electrospinning polyhydroxyalkanoate fibrous Scaffolds with antibacterial and angiogenesis effects for accelerating wound healing. *ACS Appl Mater Interfaces*. 2023;15(1):364–377. doi:10.1021/acsami.2c16905
29. Chen R, Yu J, Gong HL, et al. An easy long-acting BMP7 release system based on biopolymer nanoparticles for inducing osteogenic differentiation of adipose mesenchymal stem cells. *J Tissue Eng Regen Med*. 2020;14(7):964–972. doi:10.1002/term.3070
30. Yin X, Xia W, Fan H, et al. Nanoclay reinforced integrated Scaffold for dual-lineage regeneration of cartilage and subchondral bone. *ACS Appl Mater Interfaces*. 2024. doi:10.1021/acsami.4c07092
31. Hu H, Dong L, Bu Z, et al. miR-23a-3p-abundant small extracellular vesicles released from Gelma/nanoclay hydrogel for cartilage regeneration. *J Extracell Vesicles*. 2020;9(1). doi:10.1080/20013078.2020.1778883

32. Ramnarine-sanchez RS, Kanczler JM, Evans ND, Oreffo ROC, Dawson JI. Self-assembly of structured colloidal gels for high-resolution 3D micropatterning of proteins at scale. *Adv Mater*. 2023;2304461:1–9. doi:10.1002/adma.202304461
33. Cao B, Lin J, Tan J, et al. 3D-printed vascularized biofunctional scaffold for bone regeneration. *Int J Bioprinting*. 2023;9(3):702. doi:10.18063/ijb.702
34. Yao Q, Fuglsby KE, Zheng X, Sun H. Nanoclay-functionalized 3D nanofibrous scaffolds promote bone regeneration. *J Mater Chem B*. 2020;8 (17):3842–3851. doi:10.1039/c9tb02814e
35. Cai W, Mao S, Wang Y, et al. An engineered hierarchical hydrogel with immune responsiveness and targeted mitochondrial transfer to augmented bone regeneration. *Adv Sci*. 2024;2406287:1–13. doi:10.1002/advs.202406287
36. Wang D, Wang Y, Song D, et al. Microgels-encapsulated magnesium / Emodin-based metal organic framework nanorods for diabetic bone regeneration. *Chem Eng J*. 2024;487(January):150585. doi:10.1016/j.cej.2024.150585
37. Xie M, Sun Y, Wang J, et al. Thermo-sensitive sacrificial microsphere-based bioink for centimeter-scale tissue with angiogenesis. *Int J Bioprinting*. 2022;8(4):15–30. doi:10.18063/ijb.v8i4.599
38. Li J, Li L, Wu T, et al. An injectable thermosensitive hydrogel containing resveratrol and dexamethasone-loaded carbonated hydroxyapatite microspheres for the regeneration of osteoporotic bone defects. *Small Methods*. 2024;8(1):1–17. doi:10.1002/smtd.202300843
39. Xu JH, Chen R, Wang YD, Luo GS. Controllable gas/liquid/liquid double emulsions in a dual-coaxial microfluidic device. *Lab Chip*. 2012;12 (11):2029–2036. doi:10.1039/c2lc21193a
40. Luo J, Chen H, Wang G, Lyu J, Liu Y, Lin S. CGRP-loaded porous microspheres protect BMSCs for alveolar bone regeneration in the periodontitis microenvironment. *Adv Healthcare Mater*. 2023;2301366(639):1–13. doi:10.1002/adhm.202301366
41. Wei D, Dao J, Chen G. A micro-Ark for cells: highly open porous polyhydroxyalkanoate microspheres as injectable Scaffolds for tissue regeneration. *Adv Mater*. 2018;30. doi: 10.1002/adma.201802273
42. Vo TN, Shah SR, Lu S, et al. Injectable dual-gelling cell-laden composite hydrogels for bone tissue engineering. *Biomaterials*. 2016;83:1–11. doi:10.1016/j.biomaterials.2015.12.026
43. Zheng J, Li X, Zhang F, et al. Targeting osteoblast-osteoclast cross-talk bone homeostasis repair microcarriers promotes intervertebral fusion in osteoporotic rats. *Adv Healthc Mater*. 2024;2402117:1–13. doi:10.1002/adhm.202402117
44. Hwang HS, Lee CS. Nanoclay-composite hydrogels for bone tissue engineering. *Gels*. 2024;10(8). doi:10.3390/gels10080513
45. Castanheira EJ, Rodrigues JMM, Mano JF. Cryogels composites: recent Improvement in bone tissue engineering. *Nano Lett*. 2024;24:13875–13887. doi:10.1021/acs.nanolett.4c03197
46. Yu L, Tian Y, Ding Y, Chi Z, Liu C. Chitosan/β-glycerophosphate porous microsphere prepared by facile water-in-water emulsion as a topical hemostatic material. *Int J Biol Macromol*. 2024;277(P1):133683. doi:10.1016/j.ijbiomac.2024.133683